Radiological Physics and Technology (2019) 12:201–209
https://doi.org/10.1007/s12194-019-00506-w

Estimation and validation of the frequency responses of a scanner system and an image reconstruction system in X-ray computed tomography

Kazuhiro Sato[1] · Ryota Kageyama[2] · Yu Tomita[2] · Yumi Takane[3] · Haruo Saito[1]

Received: 24 October 2018 / Revised: 5 March 2019 / Accepted: 5 March 2019 / Published online: 21 March 2019
© Japanese Society of Radiological Technology and Japan Society of Medical Physics 2019

Abstract
In computed tomography, factors that theoretically affect the modulation transfer function (MTF) in the region near the isocenter are the frequency responses of the scanner system (MTF_S) and reconstruction processing (MTF_A). Although MTF_S and MTF_A are performance indices that are not disclosed to the users, both can be estimated by the measured MTF with the use of theoretical formulas. In this study, we proposed two methods to obtain the MTF_S and MTF_A, and confirm their validity. The first method to obtain the MTF_S and MTF_A uses a theoretical formula and the measured MTF. Another method uses the measured MTF and the noise power spectrum. In both the methods, the MTF_S and MTF_A were obtained separately. By our proposed methods, performance indices that are not usually disclosed to the users can be known.

Keywords Computed tomography · Modulation transfer function · Noise power spectrum · Image reconstruction · Frequency response

1 Introduction

The modulation transfer function (MTF) [1, 2] and noise power spectrum (NPS) [3–5] are the physical image quality indices that are commonly used with respect to computed tomography (CT) images. The MTF and NPS are indices of resolution and noise characteristics, respectively. When these indices are used to evaluate image quality, a necessary prerequisite is that the image to be evaluated should retain linearity. A standard reconstruction algorithm for CT images is a filtered back projection (FBP), which is theoretically a linear algorithm. Therefore, the MTF and NPS are often used as physical image quality indices of a CT image reconstructed by FBP.

✉ Kazuhiro Sato
satok@med.tohoku.ac.jp

[1] Tohoku University Graduate School of Medicine, 2-1 Seiryo-machi, Aoba-ku, Sendai, Miyagi 980-8575, Japan

[2] Tohoku University School of Medicine, 2-1 Seiryo-machi, Aoba-ku, Sendai, Miyagi 980-8575, Japan

[3] Tohoku University Hospital, 1-1 Seiryo-machi, Aoba-ku, Sendai, Miyagi 980-8574, Japan

In the region near the isocenter, the main factors affecting the MTF and NPS are the frequency responses of the scanner system and the reconstruction processing [6], denoted as MTF_S and MTF_A, respectively. The MTF_S is the resolution characteristic due to the geometrical specifications of the CT scanner, and is given by the product of the frequency responses of the focal spot width and the detector aperture width. On the other hand, the MTF_A is a frequency response which is the product of a reconstruction kernel (Fourier transform of a convolution function) and the interpolation processing of projection data. As stated in Sect. 2, theoretically, the MTF obtained at the region near the isocenter is the product of MTF_S and MTF_A. In contrast, the NPS is theoretically dependent on the MTF_A, but not on the MTF_S.

By separately obtaining the MTF_S and MTF_A, it is possible to evaluate the inherent performance of the CT scanner. In addition, it is possible to verify a part of the reconstruction processing, that is otherwise difficult to confirm at the user level. In other words, confirming that the image quality behavior follows the theory helps in theoretically understanding the complex image reconstruction processing in the commercial CT scanners. For example, although the frequency characteristic of the reconstruction kernel is not disclosed to users, it is possible to determine it using the MTF_A and the theoretical formulas. It is also expected to

be applicable to various fields such as verification of actual measurement results and creation of simulated images.

As mentioned above, although the MTF_S and MTF_A are performance indices that are not disclosed to users, these can be separately calculated based on the fact that FBP is a linear computation, and the hypothesis that the image quality behavior of the current commercial CT scanners follows the theory presented previously [6–9]. The theoretical formulas related to the MTF, MTF_S, and MTF_A, as well as the NPS and MTF_A have been presented previously [3, 6, 9].

Based on the theoretical formulas, the MTF_S and MTF_A can be separately obtained with two methods. The first method can be implemented as follows. First, the MTF and NPS are measured accurately. The MTF_S is then calculated by multiplying the frequency responses of the focal spot width and the detector aperture width; the MTF_A is afterward calculated by dividing the measured MTF by the MTF_S. An alternative method uses the theoretical formulas and the measured MTF and NPS, from which the MTF_S and MTF_A are then calculated.

In this study, we propose two methods to separately calculate the MTF_S and MTF_A. We confirmed their validity by calculating the relative error of the results obtained by the two methods. In addition, the accuracy of our methods was validated in an indirect manner by comparing the calculated NPS to the measured NPS. Finally, we have discussed whether the image quality behavior of the current commercial CT scanners is consistent with the theory presented previously.

2 Materials and method

2.1 Theoretical formulas

The MTF is the product of the non-algorithmic and algorithmic frequency responses. Mathematically, the MTF in the region near the isocenter can be expressed as shown in Eq. (1) [6]:

$$\mathrm{MTF}(f) = \mathrm{MTF_S}(f) \cdot \mathrm{MTF_A}(f), \tag{1}$$

where f is the spatial frequency, and $MTF_S(f)$ is the non-algorithmic frequency response of the CT scanner. The MTF_S is the response inherent to the CT scanner, and is defined by the focal spot width and the detector aperture width as described later. $MTF_A(f)$ is the frequency response of the image reconstruction algorithm. The MTF_A is affected by the image reconstruction kernel, denoted by $H(f)$ [9], and also by the frequency response of the interpolation operation for back projection, denoted by $I(f)$. The interpolation of the projection data is the process to convert discretely arranged projection data into continuous data before back projection. Since this process must be a linear interpolation, its frequency response $I(f)$ can be expressed as follows [6, 10]:

$$I(f) = \left(\frac{\sin(\pi f \Delta t)}{\pi f \Delta t} \right)^2, \tag{2}$$

where Δt denotes the ray pitch. In reality, the frequency response of the image reconstruction algorithm is affected by both $H(f)$ and $I(f)$. Therefore, the essential reconstruction kernel $G(f)$ is the product of $H(f)$ and $I(f)$. The relationship between MTF_A and $G(f)$ is as follows [6, 9]:

$$\mathrm{MTF_A}(f) = \frac{H(f)I(f)}{|f|} = \frac{G(f)}{|f|}. \tag{3}$$

To improve the resolution, the ray pitch should be infinitesimal. However, in practice, the ray has a certain width due to the spreading of the focal spot width, W_F and the detector aperture width W_D. Blur depends on the focal spot width at the isocenter, W'_F and the detector aperture width at the isocenter, W'_D. W'_F and W'_D are given by:

$$W'_F = W_F \cdot \frac{R_{FD} - R_F}{R_{FD}}, \tag{4}$$

$$W'_D = W_D \cdot \frac{R_F}{R_{FD}}, \tag{5}$$

where R_{FD} is the distance between the source and the detector, and R_F is the distance between the source and the isocenter.

At the ray position t, the profile $B_D(t)$ in the t direction of the X-ray beam depends on the detector aperture width at the isocenter, and is a rectangular function. $B_D(t)$ can be expressed by the following equation [7]:

$$B_D(t) = \begin{cases} 1, & |t| < W'_D \\ 0, & \text{eleswhere} \end{cases}. \tag{6}$$

Similarly, the profile $B_F(t)$ of the X-ray beam depends on the focal spot width at the isocenter and is a rectangular function. $B_F(t)$ can be expressed by the following equation:

$$B_F(t) = \begin{cases} 1, & |t| < W'_F \\ 0, & \text{elsewhere} \end{cases}. \tag{7}$$

The Fourier transforms of $B_D(t)$ and $B_F(t)$ are the detector aperture width MTF_D and the focal spot width MTF_F, respectively. MTF_D and MTF_F are given by:

$$\mathrm{MTF_D}(f) = \frac{F\left[B_D(t)\right]}{\left(F\left[B_D(t)\right]\right)\Big|_{f=0}} = \frac{\sin\left(\pi f W'_D\right)}{W'_D}, \tag{8}$$

$$\mathrm{MTF_F}(f) = \frac{F\left[B_F(t)\right]}{\left(F\left[B_F(t)\right]\right)\Big|_{f=0}} = \frac{\sin\left(\pi f W'_F\right)}{W'_F}, \tag{9}$$

where F denotes the one-dimensional (1D) Fourier transform. $\mathrm{MTF_D}(f)$. and $\mathrm{MTF_F}(f)$ are the frequency responses of detector aperture and focus size, respectively. The X-ray beam profile $B(t)$ in the t direction is the convolution of $B_\mathrm{D}(t)$ and $B_\mathrm{F}(t)$:

$$B(t) = B_\mathrm{D}(t) * B_\mathrm{F}(t), \tag{10}$$

where $*$ denotes 1D convolution.

The Fourier transform of $B(t)$ expresses the $\mathrm{MTF_S}$. Using the convolution theorem, $\mathrm{MTF_S}(f)$ can be calculated by the following equation [6]:

$$\mathrm{MTF_S}(f) = \frac{F\,[B(t)]}{(F\,[B(t)])|_{f=0}} = \frac{\sin\left(\pi f W'_\mathrm{D}\right)}{W'_\mathrm{D}} \cdot \frac{\sin\left(\pi f W'_\mathrm{F}\right)}{W'_\mathrm{F}}. \tag{11}$$

Thus, the $\mathrm{MTF_S}$ can be calculated using W'_F and W'_D.

Consolidating Eqs. (1) and (11), the $\mathrm{MTF_A}$ can be calculated by the following equation:

$$\mathrm{MTF_A}(f) = \mathrm{MTF}(f) \cdot \frac{W'_\mathrm{D}}{\sin\left(\pi f W'_\mathrm{D}\right)} \cdot \frac{W'_\mathrm{F}}{\sin\left(\pi f W'_\mathrm{F}\right)} \tag{12}$$

Therefore, the $\mathrm{MTF_A}$ can be calculated from W'_F, W'_D, and the measured MTF.

The image noise is mainly determined by the image reconstruction process [8]. When the number of detected photons is approximately the same for all views and all rays, the NPS in the region near the isocenter is given by the following equation [3, 9]:

$$\mathrm{NPS}(f) = \frac{\pi}{M_\mathrm{view}\bar{N}} \cdot \frac{|G(f)|^2}{f}, \tag{13}$$

where M_view denotes the number of views used for the image reconstruction, and $\bar{N}$ denotes the mean number of detected photons. Substituting Eqs. (3) into (13), we obtain the following equation:

$$\mathrm{NPS}(f) = \frac{\pi}{M_\mathrm{view}\bar{N}} \cdot |f| \cdot \left|\mathrm{MTF_A}(f)\right|^2. \tag{14}$$

Equation (14) shows that the NPS is defined by the $\mathrm{MTF_A}$, and is not affected the $\mathrm{MTF_S}$. By transposing Eq. (14), the $\mathrm{MTF_A}$ can be calculated from the measured NPS:

$$\mathrm{MTF_A}(f) = \sqrt{\frac{M_\mathrm{view}\bar{N}}{\pi} \cdot \frac{\mathrm{NPS}(f)}{|f|}}. \tag{15}$$

$\mathrm{SNR}(f)$, which represents the frequency characteristics of the signal-to-noise ratio (SNR), can be calculated from the measured MTF and NPS. The SNR can be defined with the following equation [11]:

$$\mathrm{SNR}^2(f) = C \cdot \frac{\mathrm{MTF}^2(f)}{\mathrm{NPS}(f)}, \tag{16}$$

where C is a coefficient depending on the scanning conditions and the test object. C can, in fact, be ignored because we intend to evaluate the difference of the frequency characteristics between the measured SNR and the estimated SNR using the same projection data. Therefore, Eq. (16) can be rewritten as:

$$\mathrm{SNR}^2(f) = \frac{\mathrm{MTF}^2(f)}{\mathrm{NPS}(f)}. \tag{17}$$

By transposing Eq. (1) and substituting this into Eq. (15) together with Eq. (14), Eq. (17) can be rewritten as:

$$\begin{aligned}\mathrm{SNR}(f) &= \sqrt{\frac{M_\mathrm{view}\bar{N}}{\pi} \cdot \frac{\left\{\mathrm{MTF_A}(f) \cdot \mathrm{MTF_S}(f)\right\}^2}{|f|\left|\mathrm{MTF_A}(f)\right|^2}} \\ &= \sqrt{\frac{M_\mathrm{view}\bar{N}}{\pi}} \cdot \frac{\mathrm{MTF_S}(f)}{\sqrt{|f|}}.\end{aligned} \tag{18}$$

The SNR thus only depends on $\mathrm{MTF_S}$ and not on $\mathrm{MTF_A}$.

2.2 Data acquisition and image reconstruction

We used a 64-channel multi-detector row CT (MDCT) system, Aquilion™ 64 (Aquilion 64; Canon Medical Systems, Tokyo, Japan) in this study. All images used to measure the MTF and NPS were acquired by a non-helical scan. The number of acquisition rows and slice thickness were 4 and 0.5 mm, respectively, with 0.5 s rotation time. All images were reconstructed using a conventional FBP algorithm, and the image matrix had a resolution of 512×512 pixels. We used the standard-type reconstruction kernel FC13 and the edge enhancement-type reconstruction kernel FC30. To preserve linearity, optional functions such as artifact suppression processing due to insufficient dose [12, 13] and non-linear image quality improvement processing [14, 15] were not used.

2.3 MTF measurement

We obtained the MTF by the point spread function (PSF) method. Module CTP528 of the CATPHAN 600 phantom (The Phantom Laboratory, Salem, New York) was scanned to obtain the PSF image. The material surrounding the bead was similar to water, allowing to accurately measure the MTF of the edge enhancement-type reconstruction kernel. The bead was positioned 20 mm away from the isocenter. Other acquisition parameters were as follows: 120 kV, 300 mA, rotation time of 0.5 s, volume CT dose index of 6.6 mGy, small focal spot (0.9×0.8 mm), slice thickness of 0.5 mm, and scan field of view (FOV) of 320 mm. The bead was imaged with a display field of view (DFOV) of 50 mm, resulting in pixel sizes of 0.0977 mm×0.0977 mm. The slice

thickness was set to 0.5 mm so that the bead was not affected by the partial volume effect. For each measurement condition, 80 images were averaged to decrease the image noise.

To measure the MTF, a region of interest (ROI) of 128 × 45 pixels was defined around the bead. The PSF was integrated to yield the line spread function (LSF), and the background pixel value was subtracted from the LSF. The background pixel value was estimated from the mean pixel value of a rectangular ROI, which was set slightly away from the bead. Afterward, the LSF was 1D fast Fourier transformed and normalized by the value of the zero frequency to obtain the MTF. Hereafter, we denote the measured MTF as $MTF_{measured}$.

2.4 NPS measurement

The NPS was obtained from the noise image of the CATPHAN uniform module (CTP 486). Acquisition parameters were the same as those of the bead scan. The uniform module was imaged with a DFOV of 150 mm. This resulted in pixel sizes of 0.2930 mm × 0.2930 mm, and a slice thickness of 1.0 mm. The noise images included structured noise, which must be removed to measure the NPS accurately [5]. To remove structured noise, the noise image was subtracted from another noise image acquired from the same detector row. To restore the quantum noise level of the subtracted image to the level before the subtraction, the subtracted image was divided by the square root of 2.

The NPS was calculated from the subtracted images using the following procedure: first, a measurement region $n(x, y)$ of 256 × 256 pixels, where x and y are the real space coordinates, was set at the center of the noise image. To maintain accuracy, particularly in the lower-frequency region, $n(x, y)$ was multiplied by the Welch-type window function $w(x, y)$ [16] given by:

$$w(x,y) = \left\{1 - \frac{x - X/2}{X/2}\right\}^2 \cdot \left\{1 - \frac{y - Y/2}{Y/2}\right\}^2 \tag{19}$$

where X and Y denote the lengths in the x-direction and y-direction of the $n(x, y)$, respectively. After $n(x, y)$ was multiplied by $w(x, y)$, the two-dimensional (2D) NPS was calculated by:

$$NPS_{2D}(u,v) = |F\{n(x,y) \cdot w(x,y)\}|^2, \tag{20}$$

where u and v are 2D coordinates of the frequency space. They are related to f as shown below:

$$f = \sqrt{x^2 + y^2}. \tag{21}$$

The 1D NPS was obtained by averaging the 2D NPS in the circumferential direction. For this circumferential averaging, a binning process with a bin size of 0.25 cycles/mm was used. To reduce the statistical error, the NPS of 160 subtracted images was measured and the results were averaged to obtain the final 1D NPS, as it is necessary to improve the measurement accuracy of the NPS in the low-frequency region to separately and accurately calculate the MTF_S and MTF_A. Theoretically, the NPS value at zero frequency is zero. However, in the preliminary measurement, the NPS value at zero frequency was not zero even when we measured the NPS using the Welch-type window function. Therefore, the measured NPS value was adopted in the frequency region above 0.05 cycles/mm. In the frequency region below 0.05 cycles/mm, the NPS value was obtained by linear interpolation. Hereafter, we denote the measured NPS as $NPS_{measured}$.

2.5 SNR calculation

Although the SNR is generally used to evaluate system performance [11], we calculated the SNR to separately obtain the MTF_S and MTF_A, and to confirm the measurement accuracy. The SNR was calculated for each reconstruction kernel from $MTF_{measured}$ and $NPS_{measured}$ using Eq. (17). Hereafter, we denote the measured SNR as $SNR_{measured}$.

2.6 Derivation and confirmation of MTF_S and MTF_A

The MTF_S and MTF_A were obtained for each reconstruction kernel using two methods. Table 1 shows the geometrical specifications of the CT scanner used in this study. The first way to obtain the MTF_S and MTF_A consisted the calculation of the focus width and the detector aperture at the isocenter. Using Eq. (11), the MTF_S was obtained and denoted as $MTF_{S,estimated}$. Substituting the $MTF_{measured}$ and $MTF_{S,estimated}$ into Eq. (1), we obtained the MTF_A, denoted as the $MTF_{A,estimated}$. The second method to obtain the MTF_S and MTF_A is by substituting $SNR_{measured}$ into Eq. (18), and then normalizing by the value of the zero frequency. The MTF_S was obtained through this process. Subsequently, the MTF_A was obtained by substituting the $NPS_{measured}$ into Eq. (15), and then normalizing by the value of the zero frequency. We denoted them as $MTF_{S,measured}$ and $MTF_{A,measured}$,

Table 1 CT geometric information

Parameter name	Value (mm)
Source-to-detector distance	1072.55
Source-to-object distance	600
Focus width	0.9
Detector width	0.57

respectively. In Eq. (15), since $\bar{N}$ is canceled by the normalization processing, it is not necessary to know $\bar{N}$.

2.7 Validation of the proposed method

The validity of the proposed method was confirmed by the relative error between the estimated and the measured MTF. The relative errors were calculated for each of the MTF_S and MTF_A values and were defined with the following formulas:

$$RE_S(f)\,[\%] = \frac{MTF_{S,measured}(f) - MTF_{S,estimated}(f)}{MTF_{S,estimated}(f)} \times 100, \tag{22}$$

$$RE_A(f)\,[\%] = \frac{MTF_{A,measured}(f) - MTF_{A,estimated}(f)}{MTF_{A,estimated}(f)} \times 100, \tag{23}$$

where RE_S and RE_A denote the relative errors on the MTF_S and MTF_A, respectively.

2.8 Accuracy of the proposed method

Although the relative error can confirm the validity of the proposed method, it cannot verify the accuracy of the results obtained. We verified the accuracy of the results by comparing the $NPS_{measured}$ and the NPS calculated using the $MTF_{A,estimated}$ and Eq. (14). Each NPS was normalized by the maximum value of the NPS to compare the spectral shapes. Hereafter, we denote the NPS obtained using the $MTF_{A,estimated}$ and Eq. (14) as $NPS_{estimated}$. If the $NPS_{estimated}$ is approximately equal to the $NPS_{measured}$, the MTF_A was accurately estimated. In other words, the degree of agreement reflects the accuracy of our method.

3 Results

Figure 1 shows the $MTF_{measured}$ obtained by the PSF method with the FC13 (standard-type) and FC30 (edge enhancement-type) kernels. Figure 2 shows the $NPS_{measured}$ with the two kernels. Figure 3 shows the $SNR_{measured}$ of FC13 and FC30 obtained by substituting the $MTF_{measured}$ and the $NPS_{measured}$ into Eq. (17). The $SNR_{measured}$ of FC13 and FC30 were almost equal.

Figure 4a, b show the MTF_S of FC13 and FC30, respectively, obtained through the two methods. In both kernels, a slight difference between the $MTF_{S,estimated}$ and $MTF_{S,measured}$ was observed in the low-frequency region (0–0.3 cycles/mm). In the frequency region above 0.3 cycles/mm, the $MTF_{S,estimated}$ essentially coincided with the $MTF_{S,measured}$.

Figure 5a, b show the MTF_A of FC13 and FC30, respectively, obtained through the two methods. For FC13, as with the MTF_S, although the $MTF_{A,estimated}$ was slightly different

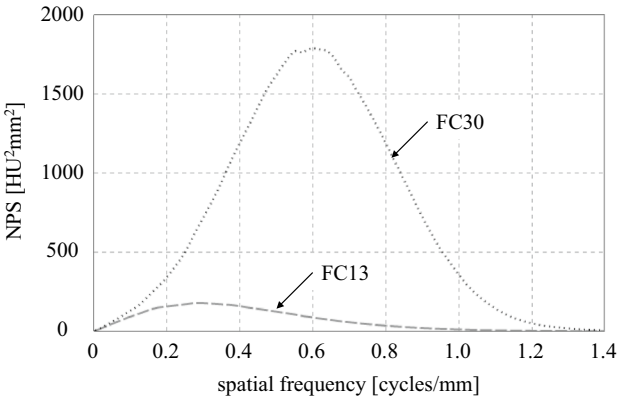

Fig. 2 NPS is obtained at the isocenter. The kernels are FC13 (dotted line) and FC30 (dashed line)

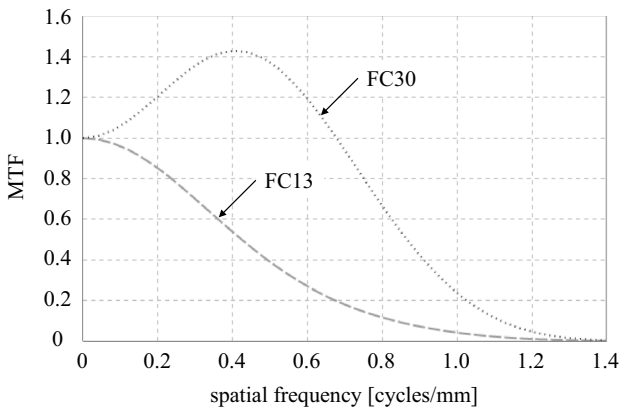

Fig. 1 MTF is obtained by the point spread function method at the isocenter. The kernels are FC13 (dotted line) and FC30 (dashed line)

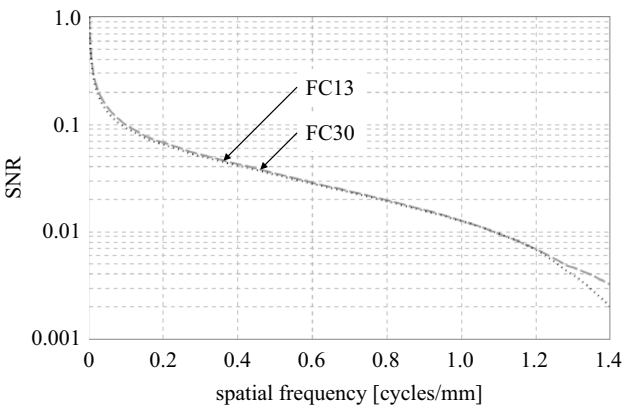

Fig. 3 SNR is obtained from Eq. (17). The kernels are FC13 (dotted line) and FC30 (dashed line)

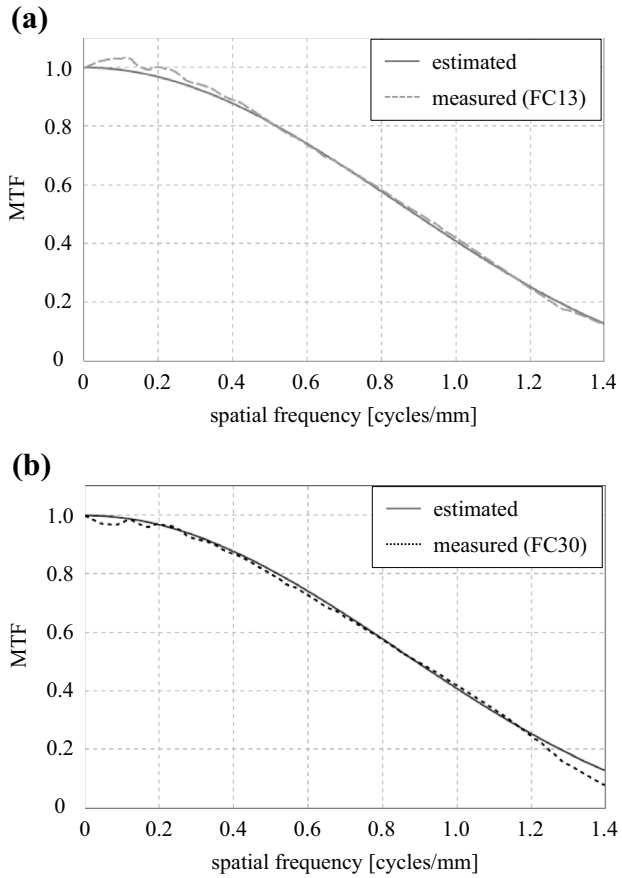

Fig. 4 $MTF_{S,estimated}$ is obtained from Eq. (11) (solid line), and $MTF_{S,measured}$ is obtained from SNR and Eq. (17) (dashed line). The kernels are FC13 (**a**) and FC30 (**b**). For FC13, $MTF_{S,measured}$ and $MTF_{S,estimated}$ coincide except in the low-frequency region. For FC30, $MTF_{S,measured}$ and $MTF_{S,estimated}$ coincide in the frequency region between 0.2 cycles/mm and 1.2 cycles/mm

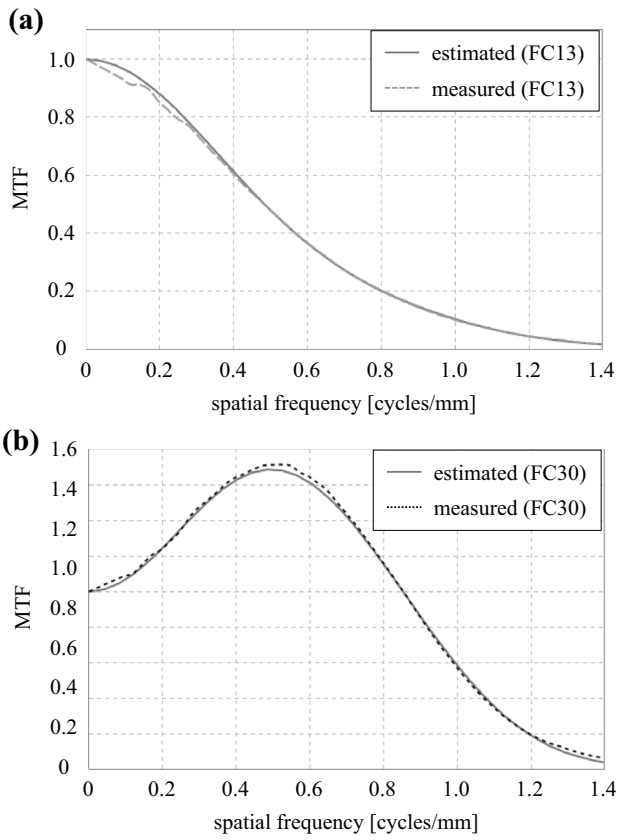

Fig. 5 $MTF_{A,estimated}$ is obtained from Eq. (12) (solid line) and $MTF_{A,measured}$ is obtained from Eq. (15) (dashed line). The kernels are FC13 (**a**) and FC30 (**b**). For FC13, $MTF_{A,estimated}$ and $MTF_{A,measured}$ coincided in the low-frequency region, above 0.4 cycles/mm. Conversely, for FC30, $MTF_{A,measured}$ is slightly higher than $MTF_{A,estimated}$ in the entire frequency region

from the $MTF_{A,measured}$ in the low-frequency region, MTF_A coincided in both the middle- and high-frequency region. For FC30, the $MTF_{A,estimated}$ essentially coincided with the $MTF_{A,measured}$.

Figure 6a, b show the relative error, and confirm the validity of the proposed method. In both the kernels, the relative error of the MTF_S was within 5% in the frequency region lower than 1.2 cycles/mm. The relative error of the MTF_A was also within 5%.

Figure 7a, b show the NPSs of FC13 and FC30, respectively, obtained with the two methods. In both the kernels, the $NPS_{measured}$ essentially coincided with the $NPS_{estimated}$.

4 Discussion

In this study, we proposed two methods to obtain the MTF_S and MTF_A and confirmed their validity by determining the relative error for each MTF. For the following reasons, the two proposed methods were shown to be valid to separately obtain the MTF_S and MTF_A. First, the values of the $SNR_{measured}$ of FC 13 and FC 30 were in agreement, which indicated high measurement accuracy. Second, the relative error was within 5% for both the MTF_S and MTF_A. Third, the accuracy of the proposed methods was validated by comparing the $NPS_{estimated}$ to the $NPS_{measured}$. In both the kernels, the $MTF_{A,estimated}$ was an accurate estimate, since the $NPS_{measured}$ coincided with the $NPS_{estimated}$. The fact that $MTF_{A,estimated}$ was an accurate estimate implies that the $MTF_{S,estimated}$ was also accurate.

The MTF_S and MTF_A can be calculated separately using the theoretical formulas and the highly accurate MTF measurement. Therefore, we confirmed that the theoretical formulas presented previously [6–10] are applicable to the current commercial CT scanner. It is known that the image quality behavior differs between the region near the isocenter and the regions far from it [11]. In the region near the isocenter, the image quality behavior is consistent with the theoretical formulas. However, in the region far from the isocenter, it

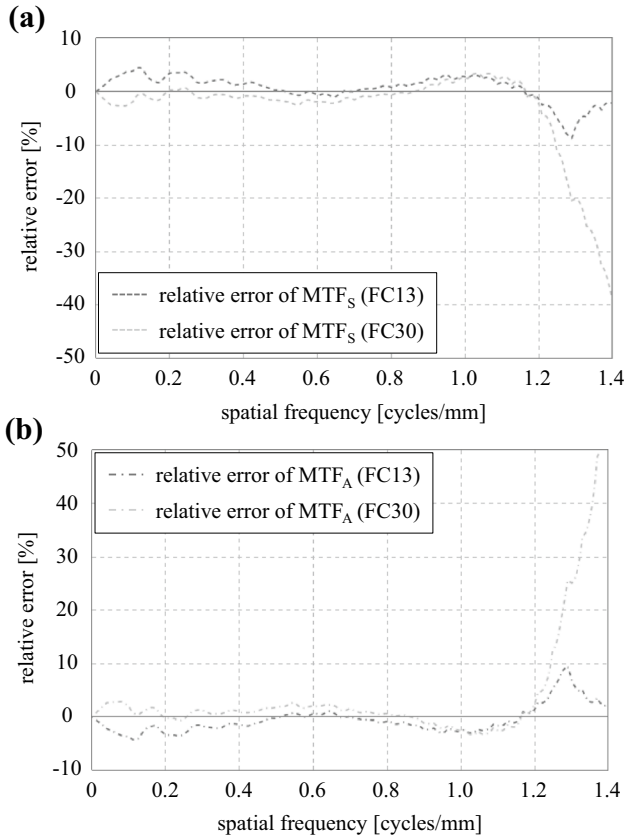

Fig. 6 Relative error between $MTF_{S,estimated}$ and $MTF_{S,measured}$ (**a**) and between $MTF_{A,estimated}$ and $MTF_{A,measured}$ (**b**). The relative error is less than 5% in the frequency region below 1.2 cycles/mm for both MTF_S and MTF_A

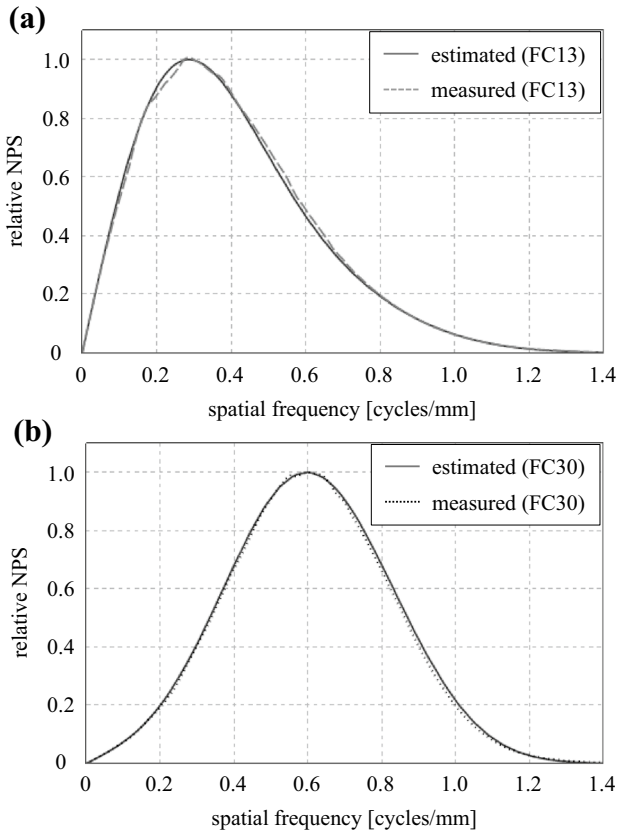

Fig. 7 The $NPS_{estimated}$ is obtained from Eq. (14), the $MTF_{A,estimated}$ (solid line), and the $NPS_{measured}$ (dashed line). The kernels are FC13 (**a**) and FC30 (**b**). The $NPS_{estimated}$ is in good agreement with the $NPS_{measured}$ in both the kernels

is necessary to include blurring factors in the theoretical formulas. There are two main causes of blurring. One is the movement of the projection ray, since the image becomes blurrier the as the distance from isocenter increases owing to an increasing influence of such a movement. The other factor responsible for blurring is the focal spot height. Similarly, the image becomes blurrier as the influence of the focal spot height increases.

When the MTF_A is obtained, it is possible to calculate the reconstruction filter kernel based on the theoretical formula. As can be seen from such a formula, while the MTF_S is inherent to the CT scanner, the MTF_A is related to the filter kernel, which drastically changes the image quality. The filter kernel cannot be calculated directly; however, it is possible to calculate the filter kernel using the theoretical formulas and the MTF_A. Our method can be used to obtain the filter kernel. In clinical practice, obtaining the filter kernel will provide information such as graininess and image noise.

The MTF_S and MTF_A could be accurately separated using the geometrical specifications of the CT scanner and the MTF measurement. Most information on geometrical specifications required in our method is disclosed by the manufacturer. Moreover, the geometrical information is included in the information tag of the image outputted in the digital imaging and communications in medicine format. The MTF_S can be calculated using this information. By obtaining the MTF_S accurately, the MTF_A can be calculated from the measured MTF.

Although the MTF_S and MTF_A could be separately obtained using the measurements of the MTF and NPS, both the $MTF_{S,measured}$ and $MTF_{A,measured}$ did not completely coincide with the $MTF_{S,estimated}$ and $MTF_{A,\,estimated}$. In other words, the accuracies of the $MTF_{S,measured}$ and $MTF_{A,measured}$ were not sufficient in the low-frequency region. This can be attributed to the difficulty faced in accurate measurement of the NPS in the low-frequency region, mainly due to the structured noise [5]. To accurately measure the NPS, we acquired the subtracted images and measured the NPS from them. However, the NPS value at the origin was not zero. Because the inaccuracy of the NPS in the low-frequency region decreases the calculation accuracy of the MTF_A, we obtained the NPS value of the very low-frequency region by an interpolation process.

Nevertheless, a relative error was still present in the low-frequency region.

In the frequency region above 1.2 cycles/mm, the relative error of both the MTF_S and MTF_A of FC30 exceeded 10% (Fig. 6). The main reason for this was the overestimation of the NPS in the high-frequency region. Since the relative error of FC13 was smaller than that of FC30, the calculation accuracy of FC13 was higher than that of FC30. On the other hand, the SNR of FC30 was lower than that of FC13 in the frequency region higher than 1.2 cycles/mm (Fig. 3). This was due to the overestimation of the NPS in the frequency region higher than 1.2 cycles/mm. The overestimation of the NPS affected the calculation accuracy of $MTF_{S,measured}$ and $MTF_{A,measured}$, which increased the relative error.

Even if the DFOVs of the PSF images and the noise images were not the same, our results could be obtained based on the theoretical formulas. The noise images that were used to measure the NPS were reconstructed with a DFOV of 150 mm. On the other hand, the bead image was reconstructed with a smaller DFOV of 50 mm. If the DFOV is less than about 150 mm, the image quality behavior should be consistent with the theory.

To separately obtain the MTF_S and MTF_A by our methods, the images that are used to calculate the MTF and NPS must retain linearity. However, the images reconstructed by iterative reconstruction and hybrid iterative reconstruction show non-linear behavior [17–21]. This is one of the central limitations of our study. The images processed by the adaptive filter also manifest non-linear behavior [22]. Moreover, artifact suppression and aliased noise reduction processing are non-linear in nature. When our methods are applied to these non-linearly processed images, the obtained MTF_A also includes the frequency response of non-linear processing in addition to the response of reconstruction processing. In this case, by measuring the frequency response of the reconstruction processing without including the response of the non-linear processing, it may be possible to obtain only the frequency response of the non-linear processing. The quotient obtained by dividing the MTF_A, which includes the frequency response of the non-linear processing by the MTF_A, which does not include the frequency response of the non-linear processing will represent only the frequency response of the non-linear processing. Thus, the calculated frequency response indicates information which is otherwise not disclosed to the user. However, the result is limited by its dependency on the test object and measurement conditions.

5 Conclusion

In this study, we proposed two methods to separately obtain the MTF_S and MTF_A. The MTF_S and MTF_A were accurately obtained using the geometrical specifications of the CT scanner and the measured MTF. In addition, this study shows that the image quality behavior of a current commercial CT scanner is consistent with the theoretical formulas presented in this study.

Acknowledgements This work was supported by JSPS KAKENHI Grant Number JP17K10391.

Compliance with ethical standards

Conflict of interest The authors declare that they have no conflicts of interest.

Ethical statement This study was not performed on animal or human samples; therefore, it does not deal with animal and human ethical issues and informed consent.

References

1. Nickoloff EL. Measurement of the PSF for a CT scanner: appropriate wire diameter and pixel size. Phys Med Biol. 1988;33:149–55.
2. Boone JM. Determination of the presampled MTF in computed tomography. Med Phys. 2001;28(3):356–60.
3. Riederer SJ, Pelc NJ, Chesler DA. The noise power spectrum in computed X-ray tomography. Phys Med Biol. 1978;23:446–54.
4. Kijewski MF, Judy PF. The noise power spectrum of CT images. Phys Med Biol. 1987;32:565–75.
5. Boedeker KL, Cooper VN, McNitt-Gray MF. Application of the noise power spectrum in modern diagnostic MDCT: part I. Measurement of noise power spectra and noise equivalent quanta. Phys Med Biol. 2007;52:4027–46.
6. Mori I, Machida Y. Deriving the modulation transfer function of CT from extremely noisy edge profiles. Radiol Phys Technol. 2009;2:22–32.
7. Glover GH, Eisner RL. Theoretical resolution of computed tomography systems. J Comput Assist Tomogr. 1979;3:85–91.
8. Chesler DA, Riederer SJ, Pelc NJ. Noise due to photon counting statistics in computed X-ray tomography. J Comput Assist Tomogr. 1977;1:64–74.
9. Wagner RF, Brown DG, Pastel MS. Application of information theory to the assessment of computed tomography. Med Phys. 1979;6:83–94.
10. Tominaga C, Azumi H, Goto M, Taura M, Homma N, Mori I. Tilted-wire method for measuring resolution properties of CT images under extremely low-contrast and high-noise conditions. Radiol Phys Technol. 2018;11:125–37.
11. Hara T, Ichikawa K, Sanada S, Ida Y. Image quality dependence on in-plane positions and directions for MDCT images. Eur J Radiol. 2010;75:114–21.
12. Hsieh J. Adaptive streak artifact reduction in computed tomography resulting from excessive X-ray photon noise. Med Phys. 1998;25:2139–47.
13. Kachelriess M, Watzke O, Kalender WA. Generalized multi-dimensional adaptive filtering for conventional and spiral single-slice, multi-slice, and cone-beam CT. Med Phys. 2001;28:475–90.
14. Wessling J, Esseling R, Raupach R, Fockenberg S, Osada N, Gerß J, et al. The effect of dose reduction and feasibility of edge-preserving noise reduction on the detection of liver lesions using MSCT. Eur Radiol. 2007;17:1885–91.
15. Kalra MK, Maher MM, Sahani DV, Blake MA, Hahn PF, Avinash GB, et al. Low-dose CT of the abdomen: evaluation of image

improvement with use of noise reduction filters-pilot study. Radiology. 2003;228:251–6.
16. Jiang H, Chen WR, Liu H. Effect of window function on noise power spectrum measurements in digital X-ray imaging. Proc SPIE. 2002;4615:91–7.
17. Richard S, Husarik DB, Yadava G, Murphy SN, Samei E. Towards task-based assessment of CT performance: system and object MTF across different reconstruction algorithms. Med Phys. 2012;39:4115–22.
18. Miéville F, Gudinchet F, Brunelle F, Bochud FO, Verdun FR. Iterative reconstruction methods in two different MDCT scanners: physical metrics and 4-alternative forced-choice detectability experiments—a phantom approach. Phys Med. 2013;29:99–110.
19. Samei E, Richard S. Assessment of the dose reduction potential of a model-based iterative reconstruction algorithm using a task-based performance metrology. Med Phys. 2015;42:314–23.
20. Silva AC, Lawder HJ, Hara A, Kujak J, Pavlicek W. Innovations in CT dose reduction strategy: application of the adaptive statistical iterative reconstruction algorithm. Am J Roentgenol. 2010;194:191–9.
21. Gervaise A, Osemont B, Lecocq S, Noel A, Micard E, Felblinger J, et al. CT image quality improvement using adaptive iterative dose reduction with wide-volume acquisition on 320-detector CT. Eur Radiol. 2012;22:295–301.
22. Okumura M, Ota T, Tsukagoshi S, Katada K. New method of evaluating edge-preserving adaptive filters for computed tomography (CT): digital phantom method. Jpn J Radiol Technol. 2006;62:971–8.

Publisher's Note Springer Nature remains neutral with regard to jurisdictional claims in published maps and institutional affiliations.